A deep learning framework to estimate elastic modulus from ultrasound measured displacement fields

Utsav Ratna Tuladhar, Richard Simon, Cristian Linte, Michael Richards

Utsav Ratna Tuladhar, Richard A. Simon, Cristian A. Linte, Michael S. Richards, "A deep learning framework to estimate elastic modulus from ultrasound measured displacement fields," Proc. SPIE 12470, Medical Imaging 2023: Ultrasonic Imaging and Tomography, 124700P (10 April 2023); doi: 10.1117/12.2654675

SPIE.

Event: SPIE Medical Imaging, 2023, San Diego, California, United States

A Deep Learning Framework to Estimate Elastic Modulus from Ultrasound Measured Displacement Fields

Utsav Ratna Tuladhar[a], Richard A. Simon[b], Cristian A. Linte[b], and Michael S. Richards[b]

[a]Electrical and Computer Engineering, Rochester Institute of Technology, Rochester, NY, USA
[b]Biomedical Engineering, Rochester Institute of Technology, Rochester, NY, USA

ABSTRACT

Ultrasound (US) elastography is a technique that enables non-invasive quantification of material properties, such as stiffness, from ultrasound images of deforming tissue. The displacement field is measured from the US images using image matching algorithms, and then a parameter, often the elastic modulus, is inferred or subsequently measured to identify potential tissue pathologies, such as cancerous tissues. Several traditional inverse problem approaches, loosely grouped as either direct or iterative, have been explored to estimate the elastic modulus. Nevertheless, the iterative techniques are typically slow and computationally intensive, while the direct techniques, although more computationally efficient, are very sensitive to measurement noise and require the full displacement field data (i.e., both vector components). In this work, we propose a deep learning approach to solve the inverse problem and recover the spatial distribution of the elastic modulus from one component of the US measured displacement field. The neural network used here is trained using only simulated data obtained via a forward finite element (FE) model with known variations in the modulus field, thus avoiding the reliance on large measurement data sets that may be challenging to acquire. A U-net based neural network is then used to predict the modulus distribution (i.e., solve the inverse problem) using the simulated forward data as input. We quantitatively evaluated our trained model with a simulated test dataset and observed a 0.0018 mean squared error (MSE) and a 1.14% mean absolute percent error (MAPE) between the reconstructed and ground truth elastic modulus. Moreover, we also qualitatively compared the output of our U-net model to experimentally measured displacement data acquired using a US elastography tissue-mimicking calibration phantom.

Keywords: Ultrasound, Elastography, Elasticity Imaging, Inverse Problem, Deep Learning

1. INTRODUCTION

Ultrasound elastography or elasticity imaging (USEI) is a powerful technique for assessing soft tissue pathology by estimating the tissue modulus distribution from images of deforming tissue.[1] In compression elastography, tissue displacement is induced by repeated compression upon the tissue surface by the US transducer itself. This leads to an inverse problem in elasticity, where the biomechanical properties of the tissue are estimated based on the measured displacement field. There are various direct[2,3] and iterative[4] approaches developed to solve this inverse problem. A statistical framework for solving this inverse problem iteratively has been described by Mohammadi *et al.*[5] Usually, these methods pose challenges in terms of real-time response and computational cost. The direct approaches, on the other hand, require solving a differential equation, which often does not have an exact analytical solution or may be intractable. Hence, iterative approaches might provide an approximate solution instead, but the exhaustive iterative process increases the total computational cost.

The FE method is a numerical approach for discretizing and solving differential equations that is commonly used to solve the forward problem, i.e., obtaining the displacement, strain or stress fields given the known material properties and boundary conditions.[6] FE methods are also typically employed to solve the inverse problem in direct and iterative approaches. Here we use a FE technique to solve the two-dimensional (plane stress) forward elastic problem from randomly generated modulus distributions and boundary conditions. The displacement and modulus fields generated from these FE models constitute the input and output training sets, respectively, for our deep learning model.

In recent years, advances in deep learning algorithms have made it possible to create a complex mapping function between the input and output images provided that there is sufficient data. Deep learning has begun

Medical Imaging 2023: Ultrasonic Imaging and Tomography, edited by
Christian Boehm, Nick Bottenus, Proc. of SPIE Vol. 12470, 124700P
 · 1605-7422 · doi: 10.1117/12.2654675

to emerge in USEI research.[7] In elastography, CNNs have been applied to reconstruct strain fields from radio-frequency data[8] and cGANs have been used to address the inverse problems in elastography.[9]

In this work, we use FE simulations to generate a dataset to train a U-net based regression architecture, subject to a mean squared error (MSE) loss function. We then apply this model to an experimental dataset acquired using a US elastography mimicking phantom. We evaluate our U-net model results from the simulated data quantitatively using the MSE and mean absolute percent error (MAPE) metrics. We also evaluated the output of our U-net model using experimental images captured using a standard US elastography tissue mimicking phantom.

2. METHODOLOGY

2.1 FE Simulation - Forward Model

The forward model entails the generation of displacement fields using FE methods. The training and testing data are generated from the forward solution of the FE models by varying the shape, size, location and magnitude of the modulus of an inclusion in a background material of constant modulus. We use a linear elastic material model to solve the boundary value problem as shown in Figure 1. The inputs for the FE model were the modulus spatial distribution, the tissue sample geometry discretized as a FE mesh, and the boundary conditions. The FE mesh consists of evenly distributed nodes on a homogeneous 128 x 128 Cartesian grid consisting of quadrilateral elements. The modulus and displacement fields are discretized at the nodal locations.

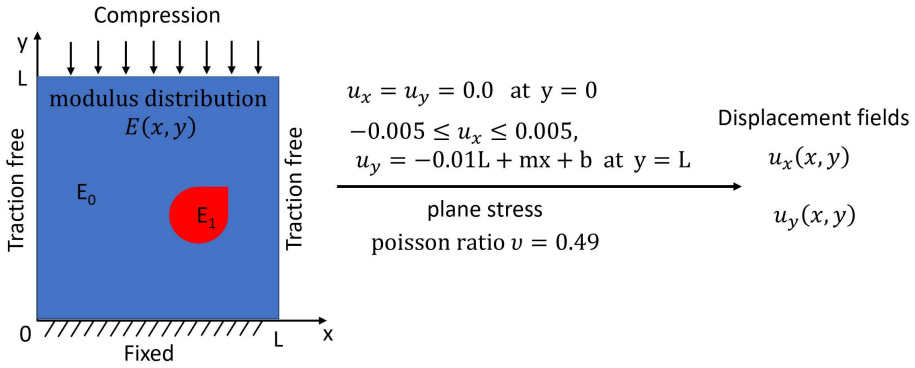

Figure 1. Generation of tissue displacement data using FEM simulations subject to known biomechanical properties (i.e. elastic modulus distribution) and prescribed boundary conditions.

As shown in Figure 1, we first construct the modulus distribution, where we vary the shape and size of every inclusion and fill them with the modulus values. For this, we start with a circle and vary the radius as a function of angle by using a sum of several cosine functions with predetermined amplitudes and phases,[10] given by the equation:

$$r(\theta) = A(1 + \sum_{n=1}^{5} B_n cos(2\pi n\theta + \psi)), \tag{1}$$

where, B_n is the amplitude that varies between $0.25 \le B_n \le 0.5$, ψ is the phase with $0 \le \psi \le 2\pi$, and A is the scaling factor with $0.113L \le A \le 0.225L$. We also vary the location of these inclusions randomly within the distribution space. A Gaussian filter, with a standard distribution uniformly between 0.5 and 4, was then applied to this modulus distribution to eliminate sharp edges. This distribution of elastic modulus was meant to mimic the variations of benign and malignant lesions typically identified during mammography screenings.

Similarly, the application of vertical compression load from the body surface can be mimicked using boundary conditions as follows. At $y = 0$, $u_x = u_y = 0.0$ as the bottom is fixed. Similarly, at $y = L$, we have $-0.005 \le u_x \le 0.005$ to account for the lateral shift of the ultrasound probe due to human error in otherwise perfect

vertical compression. Also at $y = L$, we have $u_y = -0.01L + mx + b$, where b and x_0 is chosen from a uniform random distribution within the range $-0.005 \leq b \leq 0.005$ and $0.33L \leq x_0 \leq 0.66L$, respectively, from which we also calculate $m = b/x0$. Additionally, the edges are made to be traction free. A plane stress formulation for the constitutive elasticity relation with a Poisson's ratio of 0.49 is used to mimic a linear elastic isotropic material. In this work, we use only the axial (Y direction) displacement field, u_y, to train our deep learning model.

We note that only displacement boundary conditions were utilized in the present study, and, as a result, the elastic modulus of the inclusion can only be reconstructed relative to the elastic modulus of the background tissue; essentially, the reconstructed elastic modulus of the inclusion is determined as a multiplicative factor of the background tissue elastic modulus.[11]

Since the elastic modulus is reconstructed relative to that of the background, we arbitrarily set the background modulus to unity ($E_o = 1.0$). We model two kinds of inclusions – a hard inclusion, whose modulus is greater than the modulus of the background tissue, and a soft inclusion, whose modulus is lower than that of the background. The modulus distribution for the hard inclusion lies between 1.0 and 5.0, and between 0.1 and 1.0 for the soft inclusion. As shown in Figure 2, blue represents the elastic modulus of hard inclusions, red represents the modulus of soft inclusions, and white represents the modulus of the background tissue. Furthermore, we also normalize the value of the displacement distribution from 0 to 1.

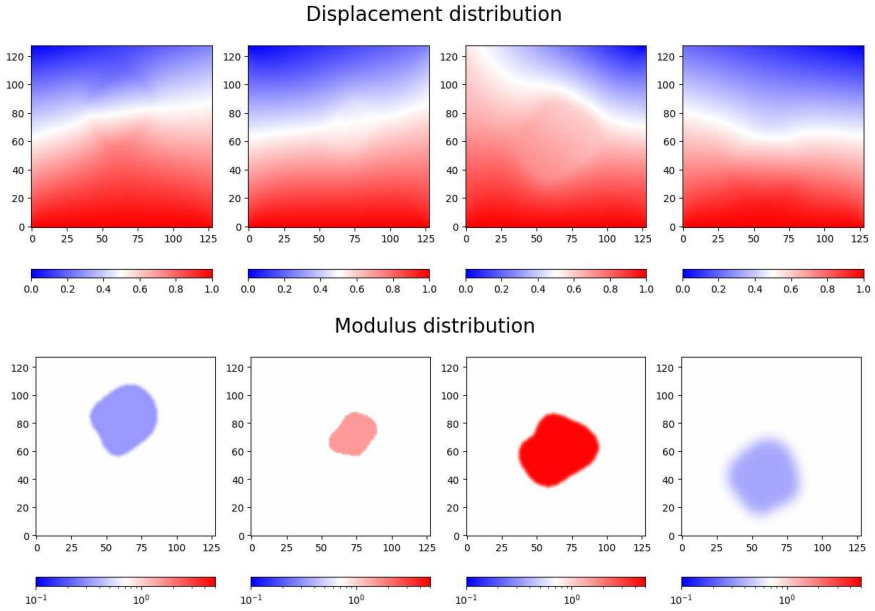

Figure 2. Examples of four simulated datasets. The tissue displacement distribution images (above) constitute the input, and the modulus distribution images (below) constitute the output. Both images are 128 x 128 pixels in size.

Our training dataset consists of 10,000 examples featuring 5050 hard inclusion and 4950 soft inclusion datasets. The test dataset features 1000 images consisting of 505 hard inclusion and 495 soft inclusion data. Moreover, we also have the 45 images from experimental data acquired using a US elastography tissue mimicking phantom.

2.2 DL Model - Inverse Problem

In our deep learning approach, we utilize a U-net architecture,[12] to learn the mapping between the displacement fields and modulus field as shown in the figure 3. Similar approach was used in the Pix-to-Pix framework[13] for image-to-image translation tasks. Unlike the typical Pix-to-Pix framework that employs both generator and discriminator components, we elect to employ only the generator component along with the mean squared error

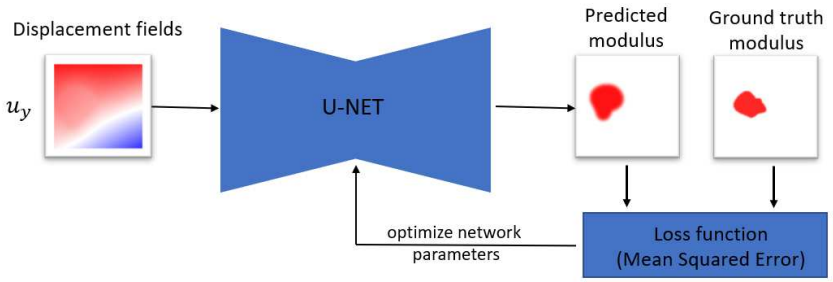

Figure 3. Deep learning U-NET model featuring a MSE loss function for optimization.

(MSE) loss function for optimization. The MSE loss function is calculated using:

$$MSE = \frac{1}{N_{pixels}} \sum_{i=1}^{N_{pixels}} (E_i^t - E_i^p)^2, \tag{2}$$

where N_{pixels} is the number of pixel, to calculate the loss function between the predicted E_i^p and the ground truth E_i^t modulus.

We used a batch size of 32, with 100 epochs and an Adam optimizer with a learning rate of 2×10^{-4}. For data pre-processing, we normalization the displacement fields to values between 0 and 1. In addition to optimizing, we also used the MSE metric for the evaluation of simulated data. Furthermore, we also calculated the mean absolute percentage error (MAPE) metric:

$$MAPE = \frac{1}{N_{pixels}} \sum_{i=1}^{N_{pixels}} \left| \frac{E_i^t - E_i^p}{E_i^t} \right|, \tag{3}$$

which returns a normalized and more intuitive metric of modulus accuracy.

2.3 Phantom Experiments

In compression elastography, the operator exerts manual compression on the tissue using the ultrasound transducer. We collected ultrasound data at two different compression states using a tissue mimicking elasticity Phantom (Elasticity QA Ultrasound Phantom CIRS 049), which contains both hard and soft spheres. The displacement fields are calculated from the two ultrasound images using an image registration algorithm[14,15] and the axial displacement field u_y is used as input to the trained deep learning model to obtain the modulus predictions. For this phantom, the elastic modulus of the background was 25×10^6 KPa, 80×10^{12} KPa for the hard inclusion, and 8×10^3 KPa for the soft inclusion. Taking the ratio of inclusions with respect to background, we would have an expected the predicted modulus to be in the range of 2.19 to 4.84 for the hard inclusions and 0.16 to 0.58 for the soft inclusions.

We collected two datasets from the phantom experiment, one each for a hard and soft inclusion. We calculated the average modulus value and the contrast-to-noise (CNR) ratio[16] for these data using equation 4 below:

$$CNR = \frac{2(\hat{s_t} - \hat{s_p})^2}{\hat{\sigma_t}^2 + \hat{\sigma_p}^2}, \tag{4}$$

where $\hat{s_t}$,$\hat{s_p}$ are the mean and $\hat{\sigma_t}$, $\hat{\sigma_p}$ are the standard deviation of the inclusion and background respectively. To separate each inclusion from the background, we manually defined a circular region of interest, as shown by the dotted circles in Figure 5.

3. RESULTS AND DISCUSSIONS

3.1 Simulated Test Data

To analyse the predicted modulus images from our test data, we generated mask images that were used to separate the inclusion from the background for both the ground truth (E_i^t) and predicted (E_i^p) modulus images. The mask images are generated by binarizing the modulus images using Otsu's thresholding algorithm.[17] The masks are used to calculate the average modulus values for the ground truth ($\overline{E_i^t}$) and the predicted ($\overline{E_i^p}$), for which we also compute the relative modulus error,

$$Relative\ Modulus\ Error = \frac{|\overline{E_i^t} - \overline{E_i^p}|}{|\overline{E_i^t}|}. \tag{5}$$

We also computed the dice score which is a measure of the similarity between the ground truth and predicted masks and is given by:

$$Dice\ Score = \frac{2 * |E_i^t \cap E_i^p|}{|E_i^t| \cup |E_i^p|}. \tag{6}$$

The dice score value ranges from 0 to 1, 0 being not similar at all to 1 being exactly similar. The dice scores we obtained for hard and soft inclusion are reported in Table 1. To further estimate elastic modulus reconstruction error, we calculated the MSE and MAPE between ground truth and predicted image. The average MSE obtained was 0.0018 and the average MAPE was 1.14% for the entire test data. The average error observed for all the hard and soft inclusions is also summarized in Table 1.

Table 1. Summary of mean and standard deviation values for ground truth and reconstructed elastic modulus for hard and soft inclusions. Comparison metrics include mean squared error (MSE), mean absolute percent error (MAPE) and Dice score (measure of similarity between the ground truth and predicted inclusion geometry).

Inclusion	No. of images	Mean MSE	Mean MAPE(%)	Mean Relative Modulus Error(%)	Mean Dice Score
Hard	505	0.002 ± 0.003	0.93 ± 0.34	3.37 ± 2.18	0.98 ± 0.07
Soft	495	0.001 ± 0.001	1.34 ± 0.86	5.04 ± 5.45	0.97 ± 0.06

An example of a hard inclusion is shown in Figure 4 (left 3 panels). For this prediction, the MSE was 0.002 and MAPE was 0.91%. The ground truth average modulus value was found to be 3.877 and the predicted value was 3.875 with a relative error of 5.04%, and Dice score of 0.98. Similarly, an example of a soft inclusion is shown in Figure 4 (right 3 panels). For this prediction, the MSE was 0.0006 and MAPE was 2.04%. The ground truth average modulus was 0.504 and predicted modulus value was 0.468 with a relative error of 7.14% and a dice score of 0.97.

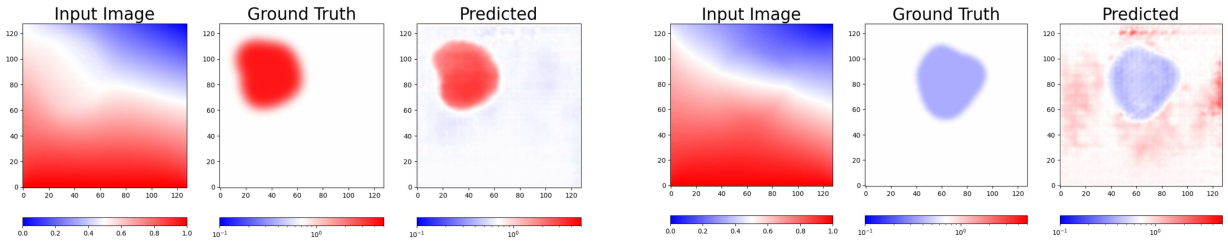

Figure 4. The ground truth and predicted modulus distribution images for hard inclusions (left 3 panels) and soft inclusion (right 3 panels).

From these results, our deep learning model is able to accurately modulus distribution from the axial displacement fields. The high dice scores indicate a high degree of overlap between the predicted and ground truth modulus location. Similarly, a low relative modulus error further supports the accuracy of the simulation results. The test results are in close agreement with the expected values and have a high level of accuracy. Moreover, this shows us that the model architecture we used is well-suited for our task and able to capture the relevant patterns in the data. Furthermore, it demonstrates that the model has been trained on a sufficient volume of data, enabling it to reach convergence towards optimal model parameter values.

3.2 Preliminary Phantom Results

Figure 5 shows the calculated axial displacement fields and predicted modulus for a hard sphere (left) with an average modulus value of 4.50 (Expected range: 2.19 to 4.84), CNR of 232.53 and a soft sphere (right) with an average modulus values of 0.40 (Expected range: 0.16 to 0.58), CNR of 15.23, both of which are within the range of the expected values.

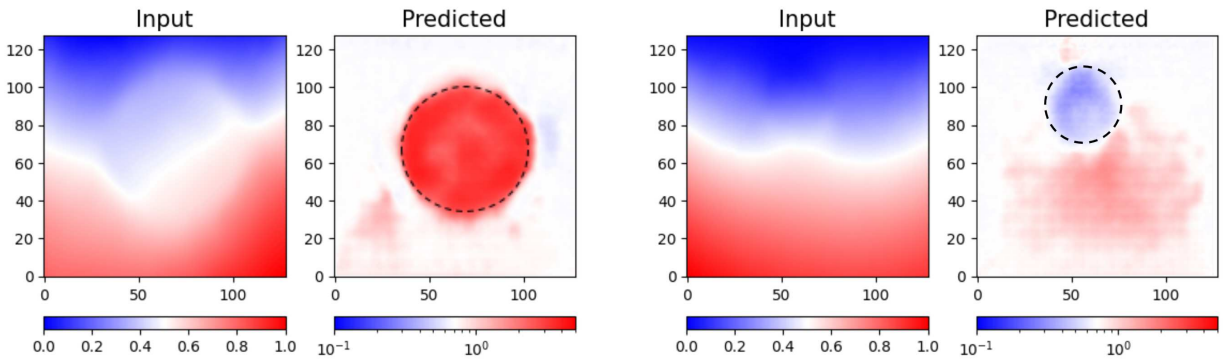

Figure 5. Elastic modulus predictions from experimental data acquired using a US elastography phantom featuring both hard (left panels) and soft inclusions (right panels).

The results in Figure 5 demonstrate that the deep learning model trained on simulated data is able to generalize to phantom data, thanks to transferable features learned from simulated data. However, we can observe some noise in the prediction of modulus distribution, which arises from the somewhat noisy input images. The noise in input image is due to error introduced by the registration algorithm we used for estimating the displacement field. Given that the simulated data is sufficiently diverse and representative of a wide variability, the algorithm trained on simulated data should generalize well to both phantom, as well as real-world clinical data. Another approach would be to add noise to the simulated data itself that would better mimic the real-world setting.

4. CONCLUSION AND FUTURE WORK

We presented a deep learning method to solve the inverse problem of finding the elastic modulus distribution in elasticity and also evaluate it's performance both quantitatively and qualitatively. We demonstrated, using FE simulated data, the development and preliminary evaluation of a deep learning approach capable of predicting the elastic modulus from both simulated and experimental US elastography data. Our preliminary results suggest that our deep learning framework can accurately predict the modulus and has the potential to be applied in real time setting as well.

For future work, we aim to apply our model to a larger phantom set for the repeatability and also to clinical data. Moreover, the training can also be conducted using both components of the displacement field. We also plan to test model accuracy with different displacement estimation techniques and also compare the deep learning approach to traditional reconstruction techniques. Additionally, we aim to improve our simulation to yield more realistic data for training that better mimics the experimental US data, and perform noise studies for sensitivity.

ACKNOWLEDGMENTS

Research reported in this publication was supported by the National Institute of General Medical Sciences Award No. R35GM128877 of the National Institutes of Health, and the Office of Advanced Cyber infrastructure Award No. 1808530 of the National Science Foundation.

REFERENCES

[1] Sigrist, R. M., Liau, J., El Kaffas, A., Chammas, M. C., and Willmann, J. K., "Ultrasound elastography: review of techniques and clinical applications," *Theranostics* **7**(5), 1303 (2017).

[2] Raghavan, K. and Yagle, A., "Forward and inverse problems in elasticity imaging of soft tissues," *IEEE Transactions on Nuclear Science* **41**(4), 1639–1648 (1994).

[3] Barbone, P., Rivas, C., Harari, I., Albocher, U., Oberai, A., and Zhang, Y., "Adjoint-weighted variational formulation for the direct solution of inverse problems of general linear elasticity with full interior data," *International Journal for Numerical Methods in Engineering* **81**, 1713–1736 (Mar. 2010).

[4] Gokhale, N. H., Barbone, P. E., and Oberai, A. A., "Solution of the nonlinear elasticity imaging inverse problem: the compressible case," *Inverse Problems* **24**(4), 045010 (2008).

[5] Mohammadi, N., Doyley, M. M., and Cetin, M., "A statistical framework for model-based inverse problems in ultrasound elastography," in [*2020 54th Asilomar Conference on Signals, Systems, and Computers*], 1395–1399 (2020).

[6] Surana, K. S. and Reddy, J. N., [*The finite element method for boundary value problems: mathematics and computations*], CRC press (2016).

[7] Li, H., Bhatt, M., Qu, Z., Zhang, S., Hartel, M. C., Khademhosseini, A., and Cloutier, G., "Deep learning in ultrasound elastography imaging: A review," *Medical Physics* (2022).

[8] Wu, S., Gao, Z., Liu, Z., Luo, J., Zhang, H., and Li, S., "Direct reconstruction of ultrasound elastography using an end-to-end deep neural network," in [*International conference on medical image computing and computer-assisted intervention*], 374–382, Springer (2018).

[9] Ni, B. and Gao, H., "A deep learning approach to the inverse problem of modulus identification in elasticity," *MRS Bulletin* , 1–7 (2020).

[10] "C++ create random shaped "blob" objects." Stackoverflow, 22 February 2019 gamedev.stackexchange.com/questions/62613/need-ideas-for-an-algorithm-to-draw-irregular-blotchy-shapes. (Accessed: 15 September 2015).

[11] Barbone, P. and Bamber, J., "Quantitative elasticity imaging: what can and cannot be inferred from strain images," *Physics in Medicine and Biology* **47**, 2147–2164 (2002).

[12] Ronneberger, O., Fischer, P., and Brox, T., "U-net: Convolutional networks for biomedical image segmentation," in [*International Conference on Medical image computing and computer-assisted intervention*], 234–241, Springer (2015).

[13] Isola, P., Zhu, J.-Y., Zhou, T., and Efros, A. A., "Image-to-image translation with conditional adversarial networks," in [*Proceedings of the IEEE conference on Computer Vision and Pattern Recognition*], 1125–1134 (2017).

[14] Richards, M. S. and Doyley, M. M., "Non-rigid image registration based strain estimator for intravascular ultrasound elastography," *Ultrasound in Medicine & Biology* **39**(3), 515–533 (2013).

[15] Chimenti, R. L., Flemister, A. S., Ketz, J., Bucklin, M., Buckley, M. R., and Richards, M. S., "Ultrasound strain mapping of achilles tendon compressive strain patterns during dorsiflexion," *Journal of Biomechanics* **49**(1), 39–44 (2016).

[16] Thitaikumar, A., Krouskop, T. A., and Ophir, J., "Signal-to-noise ratio, contrast-to-noise ratio and their trade-offs with resolution in axial-shear strain elastography," *Physics in Medicine & Biology* **52**(1), 13 (2006).

[17] Bangare, S. L., Dubal, A., Bangare, P. S., and Patil, S., "Reviewing Otsu's method for image thresholding," *International Journal of Applied Engineering Research* **10**(9), 21777–21783 (2015).